Unveiling the binding and orientation of the antimicrobial peptide Plantaricin 149 in zwitterionic and negatively charged membranes

Patricia S. Kumagai[1,†], Victor K. Sousa[2,†], Maressa Donato[2], Rosangela Itri[2], Leila M. Beltramini[2], Ana P. U. Araujo[1], Jochen Buerck[3], B. A. Wallace[4], Jose L.S. Lopes [2,*]

[1] Instituto de Física de São Carlos, Universidade de São Paulo, São Carlos, SP, 13563-120, Brasil

[2] Instituto de Física da Universidade de São Paulo, São Paulo, SP 05508-090, Brasil

[3] Karlsruhe Institute of Technology (KIT), Institute of Biological Interfaces (IBG-2), POB 3640, D-76021, Karlsruhe, Germany

[4] Institute of Structural and Molecular Biology, Birkbeck College, University of London, WC1E 7HX, UK

[†] Patricia S. Kumagai and Victor K. Sousa contributed equally to this work

* Corresponding author: Prof. Dr. Jose LS Lopes. e-mail: zeluiz@if.usp.br. Depto. Física Aplicada.

Rua do Matão 1371, São Paulo – SP, 05508-090, Brazil. Tel: +55(11)3091-7068; Fax: +55(11)3091-6706.

Acknowledgements

We are grateful for the financial support of the following: a paired Biotechnology and Biological Sciences Research Council (BBSRC) grant N012763/1/Sao Paulo Research Foundation (FAPESP) grant 2015/50347-2 (to APUA and BAW), CNPq/PIBIC fellowship (to VKS), grants 303513/2016-0 and 406429/2016-2 from CNPq-Brazil (to JLSL), FAPESP/CEPID grant 2013/07600-3 (to LMB), FAPESP grant 2018/19546-7 (to JLSL), grant P02409 from the BBSRC (to BAW). APU, JLSL, LMB, and RI are recipients of research CNPq fellowships. Access to the AU-CD at ASTRID2 was supported by a beamtime grant (to PSK and JLSL). Access to beamline UV-CD12 of the Institute of Biological Interfaces (IBG2) and the Institute for Beam Physics and Technology (IBPT) storage ring at the Karlsruhe Research Accelerator (KARA) was enabled by grants from the Karlsruhe Institute of Technology.

ORCID ID:

PS Kumagai - 0000-0001-7546-3091	R Itri - 0000-0001-9311-0804	J Buerck - 0000-0002-2256-9498
VK Sousa – 0000-0002-0430-4330	LM Beltramini - 0000-0001-5741-8238	BA Wallace - 0000-0001-9649-5092
M Donato – 0000-0002-5748-3723	APU Araujo - 0000-0001-5455-084X	JLS Lopes - 0000-0003-1281-0521

Abstract

Antimicrobial peptides are a large group of natural compounds which present promising properties for the pharmaceutical and food industries, such as broad-spectrum activity, potential for use as natural preservatives, and reduced propensity for development of bacterial resistance. Plantaricin 149 (Pln149), isolated from *Lactobacillus plantarum* NRIC 149, is a peptide with the ability to inhibit bacteria from the *Listeria* and *Staphylococcus* genera, which is capable of promoting inhibition and disruption of yeast cells. In this study, the interactions of Pln149 with model membranes composed of zwitterionic and/or anionic phospholipids were investigated using a range of biophysical techniques, including isothermal titration calorimetry, surface tension measurements, synchrotron radiation circular dichroism spectroscopy, oriented circular dichroism spectroscopy, and optical microscopy, in order to elucidate their mode of interactions and provide insight into their functional roles. In anionic model membranes, the binding of Pln149 to lipid bilayers is an endothermic process and induces a helical secondary structure in the peptide. The helices bind parallel to the surfaces of lipid bilayers and can promote vesicle disruption, depending on peptide concentration. Although Pln149 has relatively low affinity for zwitterionic liposomes, it is able to adsorb at their lipid interfaces, disturbing the lipid packing, assuming a similar parallel helix structure with a surface-bound orientation, and promoting an increase in the membrane surface area. Such findings can explain the intriguing inhibitory action of Pln149 in yeast cells whose cell membranes have a significant zwitterionic lipid composition.

Keywords: antimicrobial peptide; oriented circular dichroism spectroscopy; mechanism of action; peptide-lipid interactions; synchrotron radiation circular dichroism spectroscopy.

Introduction

Antimicrobial peptides (AMPs) are natural compounds which have been extensively studied for their potential use in the pharmaceutical industry (Kumar et al. 2018; Ageitos et al. 2017; Marshall and Arenas 2003; Bahar and Ren 2013) due to their broad spectrum of targets ranging from viruses to parasites (Gordon et al. 2005), and their reduced propensity for inducing the development of resistance by microorganisms (Bechinger and Gorr 2017). To date, a large number of AMPs produced by lactic acid bacteria have also been investigated for their potential application in the food industry as promising candidates for natural preservatives (Singh 2018; Wang et al. 2016; Rai et al. 2016), capable of inhibiting the growth of other bacteria taxonomically related to the producing strain.

The antimicrobial peptide (AMP) Plantaricin 149 (Pln149), with the sequence YSLQMGATAIKQVKKLFKKKGG (Kato et al. 1994), isolated from *Lactobacillus plantarum* NRIC149, has been described as a bacteriocin, capable of inhibiting important pathogenic bacteria such as *Listeria monocytogenes, Staphylococcus aureus, Enterococcus, Salmonella typhimurium*, with no effect on human cells. In addition, it has high sequence homology to the peptide Plantaricin A (Pln A) (Hauge et al. 1998; Sand et al. 2007) which has been described as a pheromone with anti-bacterial properties.

Previous studies performed with the synthetic amidated peptide Pln149 (Müller et al. 2007; Lopes et al. 2009), have shown that this peptide is completely unordered/unstructured in aqueous solution. However, as with many AMPs, when exerting its antimicrobial effect, Pln149 appears to adopt a highly structured form (an amphipathic α-helix) upon interaction with negatively charged lipids (Lopes et al. 2009). The electrostatic attraction between the cationic Pln149 (net charge +7 at pH 7.0) and the negative net surface charge of target bacteria is important for promoting peptide structuring and permeabilizing action on membranes, possibly through a carpet-like mechanism (Lopes et al. 2009; Sani and Separovic 2016).

Pln149 has also been demonstrated to inhibit growth and induce cell disruption in *Saccharomyces cerevisiae*, promoting severe morphological changes in the yeast cells (Lopes et al. 2009). However, yeast cell membranes, unlike the membranes of the target organisms listed above, are not predominantly comprised of negatively-charged lipids. A zwitterionic lipid composition and a complex cellular wall are found instead (Kenneth and Rose 1972), so previously proposed mechanisms/structures based on peptide adsorption and accumulation at the cell membrane guided by electrostatic attraction between the cationic peptide and the negative surface charge density at the microorganism cell membrane may not adequately explain how Pln149 impacts on *Saccharomyces* cells.

In this paper, we use a combination of biophysical methods (isothermal titration calorimetry, surface tension measurements, synchrotron radiation circular dichroism and oriented circular dichroism spectroscopies, and optical microscopy) to investigate the binding of Pln149 to different types of model membranes (monolayers, oriented lipid bilayers, and giant unilamellar vesicles). The membrane models were composed either entirely of zwitterionic phospholipids or of phospholipids with a net negative charge density. The prevalent negatively-charged lipid found in bacterial cells, phosphatidylglycerol (PG), and one of the most abundant phospholipids in eukaryotic cells, phosphatidylcholine (PC), were employed to mimic their negatively-charged and zwitterionic membrane surfaces, respectively. In addition, as *S. cerevisiae* cells usually contain low amounts of PG in their plasma membranes, and higher amounts of phosphatidylserine (PS) (Lindberg et al. 2013), the interactions of Pln149 with PS phospholipids were

also studied to better understand the potential action of the peptide on yeast cells. The results described advance our understanding of how this AMP is oriented both in negatively-charged membrane such as found in pathogenic bacteria, and in zwitterionic membranes, such as found in yeast cells.

Materials and methods

Materials – Synthetic Pln149 was produced by solid phase peptide synthesis using Fmoc chemistry, and then purified by reverse phase chromatography, as described in Lopes et al. (2009). The purity (>95%) and molecular weight (2423.7 Da) of Pln149 were determined by mass spectrometry (Lopes et al., 2009). Phospholipids 1-palmitoyl-2-oleoyl-sn-glycero-3-phosphocholine (POPC), 1-palmitoyl-2-oleoyl-sn-glycero-3-phosphoglycerol (POPG), and 1-palmitoyl-2-oleoyl-sn-glycero-3-phospho-L-serine (POPS) were purchased from Avanti Polar Lipids and reagents were P.A. grade.

High sensitivity isothermal titration calorimetry (ITC) - The partitioning of the peptide Pln149 into liposomes was examined using a high-sensitivity MicroCal VP-ITC instrument (Northampton, MA) at 25°C, using an experimental approach based on that of Seelig (2004): an aqueous solution of the peptide Pln149 (28 μM) was loaded into the sample cell (reaction volume of 1.417 mL), and multilamellar vesicles of pure POPC, pure POPG or pure POPS (vesicles at 7 mM) were injected via the titration syringe in 20 aliquots of 10 μL, under continuous stirring at 300 rpm. The change in heat rate during the titration steps was registered in real time. All the solutions were degassed under moderate vacuum (ThermoVac, Northamptom, MA, USA) prior to use, to eliminate air bubbles. The heats of dilution were determined in control experiments and subtracted from the corresponding peptide-lipid measurements. The results were analyzed using Origin 7.0 software.

Surface tension measurements – The surface activity of Pln149 was assayed with a Wilhelmy wire attached to a Delta Pi Langmuir-tensiometer (Kibron, Finland) interfaced to a computer. Measurements were made, for 30 min at 25ºC over a concentration range from 0.16 to 10 μM in pure MilliQ water. Subsequently, the adsorption kinetics of Pln149 on (separate) Langmuir monolayers of POPG, POPS, and POPC were determined by spreading a small amount of each lipid (pure POPC, POPS or POPG, and a mixture POPC/POPG 1/1 molar ratio) in methanol/hexane (10/1, v/v, at a 1 mg/mL) on top (air/water interface) of a microplate well filled with 1.2 mL MilliQ water (or containing 0.25M or 0.5 M NaCl), generating lipid monolayers at the well surface with their lateral packing density controlled from 10 to 45 mN/m. Pln149 (5.0 μM) was injected to the aqueous subphase and subsequent changes in surface pressure due to the peptide adsorption were monitored for 30 min.

Synchrotron radiation circular dichroism (SRCD) spectroscopy – The SRCD spectra of Pln149 (400 μM) were collected at the UV-CD12 (Bürck et al. 2015) beamline of the KARA synchrotron (formerly known as ANKA), Karlsruhe Institute of Technology (KIT, Germany), and at the AU-CD beamline of the ASTRID2 synchrotron at ISA (Aarhus University, Denmark). Samples were examined in aqueous solution, in the presence of 10 mM sodium dodecyl sulfate (SDS), or liposomes comprised of POPG, POPS and POPC at 1/50 peptide-to-lipid (P/L) molar ratios. The binding of the peptide to POPG liposomes was also investigated in aqueous solutions containing 0.25 M or 0.5 M sodium fluoride. SRCD spectra were measured over the wavelength range from 270 to 170 nm in either 0.5 nm or 1 nm intervals, using quartz glass Suprasil cuvettes (Hellma) with either 97 or 100 μm pathlengths, at 25°C. Baselines for each sample (containing all the components, except the peptide) were collected in the same cell. Data processing was performed using CDTool software (Lee et al. 2004) and consisted of averaging the three successive scans accumulated for each sample, subtraction of the cognate averaged baselines, smoothing with a Savitzky-Golay filter, calibration with camphorsulfonic acid, and conversion to delta epsilon units (using mean residue weights of 115.4).

Dehydrated samples were produced as follows: Aliquots (1 nmol) of Pln149 in MilliQ water were deposited on the surface of a quartz glass plate and transferred to a desiccator under moderate vacuum for 2 hours to yield a peptide film on the plate. The SRCD spectra were measured over the wavelength range from 270 to 155 nm in 1 nm intervals, at 25°C, collecting and averaging over four different rotation angles (90 degrees each, perpendicular to the direction of the beam) for each scan, in order to examine for possible orientation effects. The same quartz glass plate (without sample) was used for collecting the baseline spectrum.

Studies in lipid bilayers were done as follows: large unilamellar vesicles (LUVs) composed of either POPC or POPG, prepared by solubilizing the dried lipids in a 4/1 (v/v) chloroform/methanol mixture, evaporating the solvent under a moderate N_2 stream, followed by 2 hours in a SpeedVac system, and then rehydration by vortexing in 2 mL of aqueous solution. The multilamellar vesicles were extruded through a polycarbonate filter (100 nm pore diameter) for a minimum of 11 times to yield LUVs with an average diameter of 100 nm (the average diameter was confirmed by dynamic light scattering).

Oriented circular dichroism (OCD) *spectroscopy* – Oriented lipid bilayers were prepared as follows: aliquots of a stock solution (5 mg/mL) of either POPG, POPS, or POPC solubilized in a mixture of chloroform/methanol (1/1, v/v) were mixed with Pln149 (0.3 mg/mL) solubilized in methanol/TFE (95/5, v/v) to yield peptide-to-lipid molar ratios of 1:25, 1:50, 1:100 and 1:200 (mol/mol), and then vortexed to homogeneity. The peptide-lipid mixtures (~30-60 μL) were

slowly deposited in a circular spot of 12 mm diameter on the surface of a quartz glass Suprasil plate (Hellma) using a gastight syringe, to promote the formation of homogeneous films on the plate. The plates were then placed in a desiccator chamber kept under moderate vacuum for 2 h to ensure complete removal of the organic solvents. Prior to the measurements, the plates with the deposited samples were maintained for 16 h in a home-built OCD chamber (Bürck et al. 2008) with controlled humidity (97.6% relative humidity, maintained using a saturated solution of K_2SO_4) at 20ºC temperature to enable the rehydration of the lipid bilayers on the plate and alignment of the peptides within the oriented lipid bilayers. During the OCD measurements, the humidity and temperature within the sample cell were monitored by a capacitive relative humidity and temperature sensor (SHT 75, Sensirion, Zurich, Switzerland), which was fixed in the immediate vicinity of the sample. The cell design used is as described in Burck et al. (2008). OCD measurements were carried out on a Jasco J-810 spectropolarimeter, over the wavelength range from 260 to 180 nm, at 0.1 nm intervals, at a controlled temperature of 20ºC (above the phase transition temperature of the phospholipids), taking 2 successive spectra in 8 different positions of the plate (0, 45, 90, 135, 180, 225, 270 and 315º rotations), which were then averaged. The spectra of lipid bilayers alone were measured under the same conditions, and the averaged lipid reference spectrum was subtracted from the corresponding averaged sample spectrum. The plates were maintained under controlled humidity throughout the measurement to avoid dehydration. For each P/L ratio, at least two measurements were averaged, and finally the data of from a given series were normalized to the same spectral magnitude at the long-wavelength minimum around 220 nm.

Optical microscopy of giant unilamellar vesicles (GUVs) – GUVs composed of POPC, POPC/POPG (1/1), or POPC:POPS (1/1) containing 0.2% Rhodamine-DOPE, were produced by the electroformation method (Angelova and Dimitrov 1986). Briefly, 20 µL aliquots of a 1 mg/ml phospholipid solution in chloroform/methanol were spread on the surface of two conductive glasses coated with indium tin oxide (ITO). After solvent evaporation, a Teflon spacer was placed between the two coated glasses to form a closed chamber which was filled with the swelling solution (0.2 M sucrose). The plates were submitted to an alternating electric field of 2 V and 10 Hz frequency for 1 hour. The solution containing the GUVs was diluted 10-fold into a 0.2 M glucose solution (osmolarity measured in an Osmomat Gonotec 030 osmometer) containing increasing concentrations of Pln149 (from 16 to 250 nM). Samples were immediately observed by optical microscopy using an inverted microscope Zeiss Axiovert 200 (Jena, Germany) equipped with a Zeiss AxioCam digital camera (Jena, Germany). A Ph2 63x objective was used either in phase contrast or in fluorescent

mode (illumination with a mercury lamp HBO 103W with the filter set for excitation at 540-552nm and emission at 575-640 nm).

Results and discussion

Calorimetry studies of Pln149 binding to liposomes - ITC is a useful technique for studying peptide-lipid interactions, since it detects the heat absorbed or released during molecular interactions. The binding enthalpy reflects the overall process of peptide binding, with contributions from both the peptide adsorption and from the structuring of the lipid environment. In contrast to chemical reactions, peptide-lipid physical interactions do not involve formation/breakage of covalent bonds, and can be divided into at least three different processes: (i) electrostatic attraction of the peptide to the membrane surface; (ii) adsorption/insertion of the peptide into the polar headgroup region or into the hydrophobic core of the membrane; and (iii) conformational change of the peptide, usually associated with the initial binding process (Seelig 1997, 2004; Abraham et al. 2005; Voievoda et al. 2015). Because calorimetric measurements produce results that arise from a range of heat-generating mechanisms in peptide-lipid binding, complementary techniques are required in order to enable their interpretations.

Lipid-into-peptide titrations were used in order to evaluate the partitioning of Pln149 into model membranes with different net charges (zwitterionic POPC, and negatively charged POPG and POPS vesicles). The ITC binding isotherms of Pln149 to POPG vesicles (Figure 1a, red) displayed a typical profile of endothermic reactions, where initially each injection promoted the absorption of the heat flow (~1.1 μcal per injection). The integration of these peaks produced a calculated enthalpy of reaction (ΔH) of about 0.5 kcal/mol. The binding was of this magnitude for 7 injections, but gradually decreased until the heat of partitioning remained constant, indicating a possible saturation of Pln149-membrane interactions (at a point where all peptides in the sample cell were considered to be bound to the liposomes). Similar behavior of Pln149 was observed in POPS vesicles, but the heat of partition and, consequently, the enthalpy, was twice that obtained for POPG (Figure 1a, green). For both negatively-charged vesicles, the heat of partition was initially increased to a maximum value, and then it gradually decreased to reach the heat of dilution of the system. Such behavior could be observed for both POPG and POPS, but it was more pronounced in POPS.

The disorder-to-helix transition due to membrane interaction is a well-understood exothermic reaction (Wieprecht et al. 1999, 2000), and a large exothermic enthalpy is expected to be associated with helix formation. However, only small exothermic or even endothermic binding enthalpies are observed in most cases (Seelig 1997; Abraham et al. 2005; Wieprecht et al. 1996), because the heat for helix formation is usually compensated for other

physical processes, such as pore formation, micellization, peptide aggregation, or formation of lipid clusters (Henriksen and Andresen 2011).

In contrast, during the titration of POPC vesicles into Pln149 (Figure 1a, in blue), almost no heat change was detectable, being on the order of the dilution heat determined by vesicle titration into aqueous solution and/or aqueous solution into peptide solution. This suggests that no interactions, or only minor interactions (undetectable by the instrument), were occurring between Pln149 and the zwitterionic vesicles.

In order to check whether the Pln149 partitioning into the POPG negatively-charged vesicles was driven by electrostatic attraction, the titration of POPG vesicles into the peptide was made in a salt solution (containing 250 mM NaCl). Figure 1b shows the difference between the titration in the aqueous (red) and salt (grey) solutions: The partitioning of the peptide into POPG vesicles in the salt solution was lower than that in the aqueous solution (~0.5 μcal/injection). The heat of partition remained constant throughout the experiment (Figure 1b, grey), indicating some "competition" of the charges, i.e., the ions coming from the salt may shield the peptide and/or the membrane surface charge, thus hampering the electrostatic attraction between Pln149 and negatively-charged membranes.

Surface tension of Pln149 and its adsorption on Langmuir monolayers - The antimicrobial peptide Pln149 produced no observable surface activity over the entire concentration range from 0.16-10 μM (Figure 2a), suggesting that no peptide adsorption occurred at the air-water interface; the surface tension value monitored throughout the measured time was ~72.8 mN/m, which corresponds to the expected value for pure water. However, when a lipid monolayer was spread at the air-water interface, the peptide exhibited the ability to migrate from the subphase to the surface, thus adsorbing in the lipid monolayer. The adsorption of Pln149 onto the POPG, POPS and POPC monolayers exhibited significant changes in the lateral pressure due to the induced surface activity of Pln149 (Figure 2a). The adsorption of Pln149 on POPG and POPS monolayers produced higher values of $\Delta\pi$ than those observed for the zwitterionic phospholipid, suggesting stronger peptide-lipid interactions when electrostatic attractions are present. However, such a result on the zwitterionic POPC monolayer is clear evidence that the antimicrobial peptide was also able to migrate from the aqueous subphase to adsorb and, albeit slowly, disturb the lipid packing of an entirely zwitterionic lipid surface formed by the POPC monolayer.

Comparing the curves for the binding of Pln149 on lipid monolayers of POPG (or POPS), and POPC (Figure 2b) at different initial surface pressures (π_0), the peptide adsorption was clearly enhanced in the presence of an electrostatic attraction between the peptide and negatively charged monolayers. As the maximum insertion pressures

(MIP) of Pln149 in both POPG and POPS monolayers were determined to be ~46 mN/m, well above the value estimated for the lateral pressure of a biological membrane (30-35 mM/m) (Marsh 1996), this indicated that Pln149 is likely to be able to insert into biological membranes with a negative surface charge density. In contrast, the MIP on the zwitterionic POPC was ~35 mN/m, suggesting that the peptide Pln149 is less efficient at penetrating into zwitterionic cell membranes.

However, it can be seen that Pln149 can also interact with zwitterionic phospholipids and disturb lipid packing effectively, causing more significant changes in $\Delta\pi$ when the lipid packing of the POPC lipid monolayer was in looser molecular packing (10-25 nM/m). This is a consistent with observations that AMPs can bind defective membranes or loosely packed lipid layers of a particular lipid composition but not interact with well-formed membranes of the same lipid composition. The antimicrobial peptide TRP3 (Bozelli et al. 2012) has been reported to produce similar preferential binding to LUVs containing negatively-charged lipids, but apparently does not bind to zwitterionic vesicles, whereas it binds to micelles irrespective of their headgroup charge. The different peptide behavior of TRP3 was attributed to the predominance of intermolecular interactions (hydrophobic, hydrogen bonding, van der Waals interactions, hydration forces) other than electrostatic ones in a system where a loose molecular packing of lipids is present. Similarly to the surface behaviour of Pln149, the peptides maculatin and citropin (Ambroggio et al. 2004) interact with both zwitterionic POPC monolayers and anionic POPG bilayers, with a stronger interaction with the anionic lipid.

The action of the pheromone Plantaricin A (PlnA) on lipid membranes has also been demonstrated to be highly dependent upon lipid composition (Zhao et al, 2006). A 22-mer version of PlnA (KSSAYSLQMGATAIKQVKKLFKKWGW) (Sand et al., 2007; 2013) is a very close homolog of Pln149 (they differ only in their C-terminal residues, KGG for Pln149 and WGW for PlnA), which also presents the ability to bind to monolayers and liposomes comprised solely of zwitterionic PC lipids. However, there does not appear to be significant penetration of Pln A into these types of membranes under similar conditions. As we found for Pln149, when the negatively-charged POPG was present, the association of PlnA with lipid membranes was significantly enhanced. Interestingly, PlnA is reported to be a peptide pheromone (Kristiansen et al. 2005), which displays antimicrobial activity in addition to its pheromone activity. PlnA was first classified as a bacteriocin (an AMP) but later discovered to pheromone-like activity (Sand et al. 2010; 2013) inducing production of other plantaricin molecules in *L. plantarum* C11

SRCD spectroscopy charactering the structural properties of Pln149 bound to model membranes – SRCD spectroscopy is a valuable method for determining the spectra in the far ultraviolet and the vacuum ultraviolet wavelength ranges (the

latter at wavelengths below 200 nm where the disordered proteins/peptides structures can have a significant contribution to the spectra) (Lopes et al. 2014; Kumagai et al. 2017), was used to provide information on the protein secondary structure. The lower wavelength measurements [relative to those obtainable by conventional CD methods] not only contain additional valuable information on peptides in disordered conformations, but because of the high intensity of the light and the geometry of the instrument, also enable the examination of samples, such as membranes, which scatter light (a feature that can otherwise result in distortion of peptide spectra) (Miles and Wallace, 2016). The SRCD spectrum of Pln149 in aqueous solution (Figure 3, in black) primarily consists of a negative peak centered at 198 nm. This indicates it is predominantly in an unordered conformation.

Incubation of Pln149 with zwitterionic (POPC) or negatively-charged (POPG) liposomes produced contrasting results: while no conformational changes were observed in the Pln149 SRCD spectrum in the presence of zwitterionic vesicles (Figure 3a), an increase in the two characteristic negative peaks at 222 and 208 nm, and the appearance of a positive peak around 192 nm suggest that in the presence of POPG liposomes, the peptide includes some helical structure. In the presence of POPS, although their peak magnitudes were much smaller, these bands can also be clearly seen. A similar disorder-to-helix change also appears in the presence of the negatively-charged surfactant SDS, suggesting formation of some helical structure. Such conformational changes are consistent with the electrostatic attraction between the cationic peptide and the negative membrane, which could produce peptide re-structuring and the reported higher activity of the peptide in Gram(+) bacteria (Müller et al. 2007; Lopes et al. 2009). Helical wheel projections (Figure 3c) for residues A7 to K20 of Pln149 indicate the region with highest helical propensity and the predicted location of an amphipathic helix in the peptide.

A similar disorder-to-helix transition has previously been observed in PlnA (Hauge et al. 1998) using conventional circular dichroism spectroscopy. Those studies showed that the unstructured peptide in aqueous solution was able to adopt a helical structure in the presence of trifluoroethanol (TFE) or model membranes composed of negatively-charged phospholipids, but not in the presence of zwitterionic liposomes. This led the authors to conclude that the negative charge on the membrane is important for structuring of the similarly positively-charged PlnA peptide as an α-helix.

In order to determine whether the binding of Pln149 to the negatively-charged vesicles is driven by electrostatic attraction, the peptide was incubated with POPG vesicles prepared in salt solutions (containing 0.25 or 0.5 M of NaF). Figure 3b shows that as the concentration of NaF in the solution increased, the 222 nm band associated with helical structures was dramatically reduced, and the magnitudes and the position of the 208 nm and 192 nm bands were reduced

and shifted to 198 and 184 nm, respectively, producing peaks characteristic of disordered conformations (as seen for the peptide in aqueous solution). Thus, the partition of the peptide into the negatively-charged vesicles appears to be driven by electrostatic interactions.

The removal of bulk water from a dehydrated sample containing Pln149 (Figure 3a) also appeared to promote a similar transition from a disordered to a helical state. We propose, as it has been noticed for other disordered proteins, that this can be attributed to the removal of water molecules surrounding the peptide, favoring intramolecular hydrogen bonds rather than peptide-solvent ones (Cammers-Goodwin et al. 1996).

OCD spectroscopy to determine peptide orientation in lipid bilayers - Although the induction of the helical structure in Pln149 in the presence of negatively-charged liposomes has been revealed by its SRCD spectrum, no information about the orientation of the helix relative to the membrane bilayer direction had yet been determined. Therefore, oriented circular dichroism spectroscopy was employed to characterize the conformation of Pln149 in macroscopically-oriented lipid bilayers and to evaluate its alignment as a function of peptide concentration in such systems (using different peptide/lipid molar ratios). The OCD spectrum of Pln149 in oriented POPG bilayers (Figure 4a) at a 1/200 P/L molar ratio exhibits the two characteristic α-helix minima at 208 nm and 220 nm, but with a more pronounced minimum at 208 nm. This spectral lineshape corresponds to a surface-bound state, or simply S-state (Bürck et al. 2016), and indicates peptide insertion aligned parallel to the plane of the lipid bilayers, with the amphipathic Pln149 helix possibly intercalated at the interface between lipid head groups and the hydrophobic core of the lipid membrane. It could be speculated that the charged lysine residues point towards the aqueous phase while the leucine, isoleucine and valine residues of the hydrophobic sector of the amphipathic Pln149 helix interact with the hydrocarbon region of the model membrane.

The OCD spectra for Pln149 in POPG oriented bilayers exhibited no significant dependence on peptide concentration, i.e., P/L ratio used. When the OCD spectra were normalized to the long-wavelength minimum of this sample at 220 nm for other P/L molar ratios (up to 1/25), they also indicated the peptide orientation was in the S-state, except for the 1/25 P/L molar ratio, where the somewhat decreased intensity of the 208 nm “fingerprint” band indicated a small increase in tilt angle of the α-helix with respect to the membrane normal, suggesting a possible slight insertion of Pln149 into the lipid bilayer, but still mostly in a surface-bound state. Although at P/L molar ratios higher than 1/25 the helix tilt angle of Pln149 appeared to be further increased, assuming a more pronounced obliquely- tilted orientation (Burck et al. 2016), which is described as the T-state (not seen for any of the other molar ratios used here), this AMP

needs rather high concentrations to undergo any re-alignment, indicating that the S-state is really the most prevailing orientation of the helix in such systems. It is possible that the membrane tilt angle changing at the P/L ratio of 1/25 may be due to a crowding effect. Assuming all residues of Pln149 interact with the lipid surface (part of the residues in helical conformation and part unstructured), the whole area of the outer lipid surface is estimated to be fully covered by Pln149. Estimation of the area of the lipid surface covered by Pln149 was done from simple geometrical calculations of lipid area and area occupied by peptides. Hence, as opposed to what is seen for other AMPs like PGLa and MAP (Bürck et al. 2008), Pln149 does not have appear to have a high tendency to re-align in POPG oriented lipid bilayers. As a further note, whilst the variation of the spectral magnitude of the positive band around 190 nm can be attributed to absorption flattening effects in some samples (Miles and Wallace 2016), these variations do not affect the orientation determination, because the alignment of the peptide helices was inferred from the unperturbed band around 208 nm, whose spectral magnitude is the "fingerprint" for helix alignment in OCD measurements (Bürck et al. 2008, 2016).

A relatively similar spectrum was observed for the binding of Pln149 to POPS oriented bilayers (Figure 4b), i.e. a 208 nm band with significant negative intensity. In the averaged spectra for POPS, the 208 nm band was also slightly more intense when compared to the 222 nm band, suggesting the peptide insertion is more like that in the S-state. At the P/L ratios of 1/100, 1/50 and 1/25, alignment of the peptide is more consistent with a T-state, slightly more tilted compared to that in POPG (even at low concentration). However no pure I-state (a fully inserted transmembrane orientation) could be observed at any of the measured P/L ratios (i.e. the same as in the case for POPG). The OCD spectra of Pln149 in lipid bilayers are in agreement with the model proposed for the insertion and membrane orientation of PlnA in negatively-charged membranes (Kristiansen et al. 2005). Like the PlnA helix, the Pln149 helix is oriented parallel to the membrane with the hydrophobic residues penetrating into the hydrophobic part of the membrane and the hydrophilic residues into and partly through the membrane-water interface.

Interestingly, the OCD spectrum of Pln149 in oriented POPC bilayers clearly indicates a helical conformation for the peptide (Figure 4c), suggesting the peptide is in the S-state, and once again, there is a very small re-alignment of peptide orientation at the P/L molar ratio of 1/25, less than what was observed for the negatively-charged POPG and POPS bilayers. Therefore, at the P/L molar ratio of 1/25, the negative charge alone influences the peptide molecules to tilt a little more than in the zwitterionic POPC bilayers. In the OCD assays, the interaction of the peptide Pln149 with the zwitterionic oriented lipid bilayers was probed in a system where hardly any bulk water phase was present. In this case, the peptide bound to the model membrane and the equilibrium was shifted towards the hydrated planar lipid bilayers. That is, once the bulk water was reduced, a significant disorder-to-helix transition was observed in Pln149. Although no

evidence of the interaction of Pln149 with the zwitterionic POPC vesicles had been seen by SRCD spectroscopy in aqueous solution, such results are not contradictory, since the partitioning of Pln149 in a zwitterionic liposome environment with a large excess of bulk water (which shifts the equilibrium towards the water phase in the absence of any Coulombic interactions) and in the oriented zwitterionic bilayers are different. Such a finding has already been reported in other peptide-to-lipid systems, and the partitioning of membrane-active peptides into membrane interfaces has been shown to promote the formation of regular secondary structure (Wimley and White 1996).

Optical microscopy with giant unilamellar vesicles – GUVs composed of POPC, POPC/POPG (1:1), and POPC/POPS (1/1) were spherical in shape with an average diameter of ca. ~20-60 μm. All three types of giant vesicles without peptide were very stable, showing no perturbation after 35 min (Figure 5A-C). When a small amount of Pln149 (concentration less than 64 nM) was added to the GUV solution, there was an increase in the membrane surface area, evident in the formation of buds from the giant vesicles as the main feature of membrane-peptide interaction (Figure 5D). Interestingly, the addition of 64 nM Pln149 to either POPC/POPG (Figure 5E) or POPC/POPS (Figure 5F) GUVs promoted membrane disruption and collapse after circa 8 min. This finding is in agreement with our observation that peptide addition has a larger effect on negatively-charged membranes than on zwitterionic ones. No pore formation was observed on the vesicles prior to their disruption (Figures 5E-F).

Of note, in the range of 64 nM to 250 nM Pln149, while the GUVs composed of POPC retained emitting buds (without being disrupted), the disruption of negatively-charged giant liposomes was increased and observed to occur in shorter time periods (data not shown). The disruption of some GUVs composed entirely of POPC could only be observed with 20 μM Pln149 after 9 min of incubation with the giant vesicles (data not shown).

Conclusions

The binding of the antimicrobial peptide Pln149 to vesicles is an endothermic process that can be guided/modulated by the presence of the negative surface charge density of model membranes. Moreover, for vesicles composed exclusively of zwitterionic lipids, the partitioning of the peptide is minimal, with little or no binding detected by isothermal titration calorimetry and no conformational changes observed by SRCD spectroscopy.

In contrast, Langmuir monolayer interactions and OCD spectroscopy indicated that Pln149 can significantly adsorb onto zwitterionic lipid surfaces with loose molecular packing and with spectra consistent with mostly helical structure. The antimicrobial peptide causes pronounced disruptive effects on GUVs containing negatively-charged

phospholipid (POPG or POPS) in response to increasing peptide concentration, as is evident in the increase of surface area and buds formation in zwitterionic GUVs. Taken together, these studies indicate for the first time that the antimicrobial peptide Pln149 can interact with zwitterionic phospholipids, which could explain the previously reported peptide activity on *Saccharomyces cerevisiae* cells (Lopes et al. 2009).

The binding of Pln149 to zwitterionic model membranes may have been affected by the different membrane curvatures of the two systems used: the highly curved POPC vesicles in the SRCD and the planar POPC lipid bilayers in the OCD assays. A membrane curvature-dependent binding has previously been demonstrated for other amphipathic α-helical antimicrobial peptides, where the different behaviors on small and giant unilamellar vesicles and the differences in kinetics were attributed to the curvature dependent binding affinities (Tabaei et al. 2012; Iwamoto et al. 2007; Koller and Lohner 2014; Strandberg et al. 2012). Also, the different degrees of hydration of LUVs and oriented bilayers have been already reported to promote differences in the insertion of the AMPs aurein 1.2 and carein 1.1 in model membranes (Fernandez et al. 2013).

Membrane curvature, hydration, and lipid organization were shown to play roles in modulating the interactions of Pln149 with lipid membranes, especially in the absence of electrostatic attraction. Therefore, as the model membranes used in the Langmuir monolayers and the surface of GUVs are similar to horizontal planes for the adsorption of Pln149, insertion between the lipid headgroups appear to alter the lipid molecular packing and may induce curvature strain in the planar lipid membranes that can contribute to the formation of the curved morphologies seen by microscopy. Alternatively, bilayers formed from the unsaturated zwitterionic lipid POPC are known to present a slight negative spontaneous curvature (Strandberg et al. 2012), hence the adsorption of Pln149 within this bilayer could initially release such lipid stress, but then, as more peptide accumulates at lipid surface, the membrane lateral pressure is increased .

In the “carpet-like” model of interaction (Shai 2002), helical peptides are in contact with lipid headgroups during the whole process of membrane permeation and do not insert into the hydrophobic core of the membrane. Here, Pln149 was shown to produce such types of interactions with both negatively-charged and zwitterionic lipid headgroups. It is possible that Pln149 might use a very similar mechanism of action on Gram(+) bacteria, i.e., with the peptide accumulation at the surface of the membrane, eventually inducing an α-helix in an environment where the amount of water is reduced, and this helix is aligned parallel to the membrane surface and can realign as a function of peptide accumulation at the membrane.

The N-terminal residues of Pln149 are not expected to contribute to the electrostatic attraction of the peptide by charged membranes and are not predicted to be part of the amphipathic helix. However, this region affects the peptide

hydrophobic moment, which could contribute to the Pln149 adsorption, causing additional strain in the membrane, as the N-terminus region must be located at the lipid-aqueous interface. The participation of this segment in the action of Pln149 has previously been demonstrated (Lopes et al. 2013); it showed the reduced leakage action, an increase of minimum inhibitory concentration (MIC) values, reduced membrane binding, and a change of the peptide action from bactericidic to bacteriostatic. The modulation of Pln149 action due to its N-terminus may occur in either zwitterionic or negatively charged membranes.

Therefore, this study has suggested that a carpet-like model may be the mechanism of action for Pln149 in both types of lipid systems: either those with a negative surface charge density (such as the cell membrane of Gram(+) bacteria) or those with zwitterionic features (as in the POPC membrane models used here and in *Saccharomyces* systems).

Conflict of Interest: The authors declare that they have no conflict of interest.

References

Abraham T, Lewis RN, Hodges RS, McElhaney RN (2005) Isothermal Titration Calorimetry Studies of the Binding of a Rationally Designed Analogue of the Antimicrobial Peptide Gramicidin S to Phospholipid Bilayer Membranes. Biochemistry 44:2103–2112. https://doi.org/10.1021/bi048077d

Ageitos JM, Sánchez-Pérez A, Calo-Mata P, Villa TG (2017) Antimicrobial Peptides (AMPs): Ancient Compounds that Represent Novel Weapons in the Fight Against Bacteria. Biochem Pharmacol 133:117-138. https://doi.org/10.1016/j.bcp.2016.09.018

Ambroggio E E, Separovic F, Bowie J, Fidelio GD (2004) Surface Behaviour and Peptide-Lipid Interactions of the Antibiotic Peptides, Maculatin and Citropin. Biochim Biophys Acta 1664:31-37. https://doi.org/10.1016/j.bbamem.2004.03.013

Angelova MI and Dimitrov DS (1986) Liposome Electroformation. Faraday Discuss Chem Soc 81:303-311. http://doi.org/10.1039/DC9868100303

Bahar AA and Ren D (2013) Antimicrobial Peptides. Pharmaceuticals (Basel) 6:1543-1575. https://doi.org/10.3390/ph6121543

Bechinger B and Gorr SU (2017) Antimicrobial Peptides: Mechanisms of Action and Resistance. J. Dent. Res 96:254-260. https://doi.org/10.1177/0022034516679973

Bozelli JC, Sasahara ET, Pinto MRS, Nakaie CR, Schreier S (2012) Effect of Head Group and Curvature on Binding of the Antimicrobial Peptide Tritrpticin to Lipid Membranes. *Chem Phys Lipids* 165:365-373. https://doi.org/10.1016/j.chemphyslip.2011.12.005

Bürck J, Roth S, Wadhwani P, Afonin S, Kanithasen N, Strandberg E, Ulrich AS (2008) Conformation and Membrane Orientation of Amphiphilic Helical Peptides by Oriented Circular Dichroism. Biophys. J 95:3872-3881. https://doi.org/10.1529/biophysj.108.136085

Bürck J, Roth S, Windisch D, Wadhwani P, Moss D, Ulrich AS (2015) UV-CD12: Synchrotron Radiation Circular Dichroism Beamline at ANKA. J. Synchrotron Rad 22:844–852. https://doi.org/10.1107/S1600577515004476

Bürck J, Wadhwani P, Fanghänel S, Ulrich AS (2016) Oriented Circular Dichroism: a Method to Characterize Membrane-active Peptides in Oriented Lipid Bilayers. Acc. Chem. Res 49:184-192. http://doi.org/10.1021/acs.accounts.5b00346

Cammers-Goodwin A, Allen TJ, Oslick SL, Mcclure KF, Lee JH, Kemp DS (1996) Mechanism of Stabilization of Helical Conformations of Polypeptides by Water Containing Trifluoroethanol. J Am Chem Soc 118:3082-3090. http://doi.org/10.1021/ja952900z

Fernandez DI, Sani MA, Miles AJ, Wallace BA, Separovic F (2013) Membrane defects enhance the interaction of antimicrobial peptides, aurein 1.2 versus caerin 1.1. Biochim Biophys Acta 1828:1863-1872 https://doi.org/10.1016/j.bbamem.2013.03.010

Gordon YJ, Romanowski EG, McDermott AM (2005) A Review of Antimicrobial Peptides and their Therapeutic Potential as Anti-infective Drugs. Curr Eye Res 30:505-515. https://doi.org/10.1080/02713680590968637

Hauge HH, Mantzilas D, Moll GN,Konings WN, Driessen AJ, Eijsink VG, Nissen-Meyer J (1998) Plantaricin A is an Amphiphilic Alpha-Helical Bacteriocin-like Pheromone which Exerts Antimicrobial and Pheromone Activities through Different Mechanisms. Biochemistry 37(46): 16026-16032. http://doi.org/10.1021/bi981532j

Henriksen JR and Andresen TL (2011) Thermodynamic Profiling of Peptide Membrane Interactions by Isothermal Titration Calorimetry: A Search for Pores and Micelles. *Biophys J* 101:100-109. http://doi.org/10.1016/j.bpj.2011.05.047

Iwamoto K, Hayakawa T, Murate M, Makino A, Ito K, Fujisawa T, Kobayashi T (2007) Curvature-dependent Recognition of Ethanolamine Phospholipids by Duramycin and Cinnamycin. Biophys J 93:1608-1619. https://doi.org/10.1529/biophysj.106.101584

Kato T, Matsuda T, Ogawa E, Ogawa H, Kato H, Doi U, Nakamura R (1994) Plantaricin-149 a Bacteriocin Produced by *Lactobacillus plantarum* NRIC 149. J. Fermentation and Bioengineering 77: 277-282. https://doi.org/10.1016/0922-338X(94)90234-8

Kenneth H and Rose AH (1972) Lipid Composition of *Saccharomyces cereviseae* as Influenced by Growth Temperature. Biochim Biophys Acta – Lipids and Lipid Metabolism 260:639-653. https://doi.org/10.1016/0005-2760(72)90013-6

Koller D and Lohner K (2014) The Role of Spontaneous Lipid Curvature in the Interaction of Interfacially Active Peptides with Membranes. Biochim Biophys Acta – Biomembranes 1838:2250-2259. https://doi.org/10.1016/j.bbamem.2014.05.013

Kristiansen PE, Fimland G, Mantzilas D, Nissen-Meyer J (2005). Structure and Mode of Action of the Membrane-Permeabilizing Antimicrobial Peptide Pheromone Plantaricin A. J. Biol. Chem. 280(24): 22945-22950. http://doi.org/10.1074/jbc.M501620200

Kumagai PS, DeMarco R, Lopes JLS (2017) Advantages of Synchrotron Radiation Circular Dichroism Spectroscopy to Study Intrinsically Disordered Proteins. Eur Biophys J 46:599-606. http://doi.org/10.1007/s00249-017-1202-1

Kumar P, Kizhakkedathu JN, Straus SK (2018) Antimicrobial Peptides: Diversity, Mechanism of Action and Strategies to Improve the Activity and Biocompatibility in vivo. Biomolecules 8:4. https://doi.org/10.3390/biom8010004

Lees JG, Smith BR, Wien F, Miles AJ, Wallace BA (2004) CDtool - an Integrated Software Package for Circular Dichroism Spectroscopic Data Processing, Analysis, and Archiving. Anal Biochem 332:285–289. https://doi.org/10.1016/j.ab.2004.06.002

Lindberg L, Santos AX, Riezman H, Olsson L, Bettiga M (2013) Lipidomic Profiling of *Saccharomyces cerevisiae* and Zygosaccharomyces bailii Reveals Critical Changes in Lipid Composition in Response to Acetic Acid Stress. PLoS One 8(9):e73936. doi: 10.1371/journal.pone.0073936. eCollection 2013.

Lopes JLS, Nobre TM, Siano Á, Humpola V, Bossolan NRS, Zaniquelli MED, Tonarelli G, Beltramini LM (2009) Disruption of *Saccharomyces cerevisiae* by Plantaricin 149 and Investigation of its Mechanism of Action with Biomembrane Model Systems. Biochim Biophys Acta – Biomembranes 1788:2252-2258. https://doi.org/10.1016/j.bbamem.2009.06.026

Lopes JLS, Gómara MJ, Haro I, Tonarelli G, Beltramini LM (2013) Contribution of the Tyr-1 in Plantaricin149a to Disrupt Phospholipid Model Membranes. Int J Mol Sc 14:12313-12328. https://doi.org/10.3390/ijms140612313

Lopes JLS, Miles AJ, Whitmore L, Wallace BA (2014) Distinct Circular Dichroism Spectroscopic Signatures of Polyproline II and Unordered Secondary Structures: Applications in Secondary Structure Analyses. Protein Sci 23:1765-1772. https://doi.org/10.1002/pro.2558

Marsh D (1996) Lateral Pressure in Membranes. Biochim Biophys Acta 1286:183–223. https://doi.org/10.1016/S0304-4157(96)00009-3

Marshall SH and Arenas G (2003) Antimicrobial Peptides: a Natural Alternative to Chemical Antibiotics and a Potential for Applied Biotechnology. Electronic J Biotechnol 6:271-284. http://doi.org/10.2225/vol6-issue3-fulltext-1

Miles AJ and Wallace BA (2016) Circular Dichroism Spectroscopy of Membrane Proteins. Chem Soc Rev 45:4859-4872. http://doi.org/10.1039/C5CS00084J

Müller DM, Carrasco MS, Simonetta AC, Beltramini LM, Tonarelli GG (2007) A Synthetic Analog of Plantaricin 149 Inhibiting Food-borne Pathogenic Bacteria: Evidence for α-Helical Conformation Involved in Bacteria-membrane Interaction. J Peptide Sci 13:171-178. https://doi.org/10.1002/psc.828

Rai M, Pandit R, Gaikwad S, Kövics G (2016) Antimicrobial Peptides as Natural Bio-Preservative to Enhance the Shelf-life of Food. J Food Sci Technol 53:3381–3394. http://doi.org/10.1007/s13197-016-2318-5

Sani MA and Separovic F (2016) How Membrane-Active Peptides Get into Lipid Membranes. Acc Chem Res 49:1130-1138. http://doi.org/10.1021/acs.accounts.6b00074

Sand SL, Haug TM, Nissen-Meyer J, Sand O (2007) The Bacterial Peptide Pheromone Plantaricin A Permeabilizes Cancerous, but not Normal, Rat Pituitary Cells and Differentiates Between the Outer and Inner Membrane Leaflet. J. Membrane Biology 216(2-3): 61-71. http://doi.org/10.1007/s00232-007-9030-3

Sand SL, Oppegard C, Ohara S, Iijima T, Naderi S, Blomhoff HK, Nissen-Meyer J, Sand O (2010). Plantaricin A, a Peptide Pheromone Produced by *Lactobacillus plantarum*, Permeabilizes the Cell Membrane of Both Normal and Cancerous Lymphocytes and Neuronal Cells. Peptides 31(7): 1237-1244. http://doi.org/10.1016/j.peptides.2010.04.010

Sand SL, J. Nissen-Meyer, O. Sand and T. M. Haug (2013). Plantaricin A, a Cationic Peptide Produced by *Lactobacillus plantarum*, Permeabilizes Eukaryotic Cell Membranes by a Mechanism Dependent on Negative Surface Charge Linked to Glycosylated Membrane Proteins. Biochimica Et Biophysica Acta-Biomembranes 1828(2): 249-259. https://doi.org/0.1016/j.bbamem.2012.11.001

Seelig J (1997) Titration Calorimetry of Lipid–Peptide Interactions. Biochim Biophys Acta 1331:103–116. https://doi.org/10.1016/S0304-4157(97)00002-6

Seelig J (2004) Thermodynamics of Lipid–Peptide Interactions. Biochim Biophys Acta 1666:40–50. https://doi.org/10.1016/j.bbamem.2004.08.004

Shai Y (2002) Mode of Action of Membrane Active Antimicrobial Peptides. Biopolymers 66(4):236-48. https://doi.org/10.1002/bip.10260

Singh VP (2018) Recent Approaches in Food Bio-Preservation – a Review. Open Vet J 8:104-111. http://dx.doi.org/10.4314/ovj.v8i1.16

Strandberg E, Tiltak D, Ehni S, Wadhwani P, Ulrich AS (2012) Lipid Shape is a Key Factor for Membrane Interactions of Amphipathic Helical Peptides. Biochim Biophys Acta – Biomembranes 1818:1764-1776. https://doi.org/10.1016/j.bbamem.2012.02.027

Tabaei SR, Rabe M, Zhdanov VP, Cho NJ, Höök F (2012) Single Vesicle Analysis Reveals Nanoscale Membrane Curvature Selective Pore Formation in Lipid Membranes by an Antiviral α-Helical Peptide. Nano Lett 12:5719-5725. http://doi.org/10.1021/nl3029637

Voievoda N, Schulthess T, Bechinger B, Seelig J (2015) Thermodynamics and Biophysical Analysis of the Membrane-association of a Histidine-rich Peptide with Efficient Antimicrobial and Transfection Activities. J Phys Chem B 119:9678-9687. http://doi.org/10.1021/acs.jpcb.5b04543

Wallace BA (2009) Protein Characterisation by Synchrotron Radiation Circular Dichroism Spectroscopy. Q Rev Biophys 42:317–370. https://doi.org/10.1017/S003358351000003X

Wang S, Zeng X, Yang Q, Qiao S (2016) Antimicrobial Peptides as Potential Alternatives to Antibiotics in Food Animal Industry. Int J Mol Sci 17:603 – 615. https://doi.org/10.3390/ijms17050603

Wieprecht T, Dathe M, Schumann M, Krause E, Beyermann M, Bienert M (1996) Conformational and Functional Study of Magainin 2 in Model Membrane Environments Using the New Approach of Systematic Double-d-Amino Acid Replacement. Biochemistry 35:10844–10853. http://doi.org/10.1021/bi960362c

Wieprecht T, Apostolov O, Beyermann M, Seelig J (1999) Thermodynamics of the α-Helix-Coil Transition of Amphipathic Peptides in a Membrane Environment: Implications for the Peptide- Membrane Binding Equilibrium. J Mol Biol 294:785−794. https://doi.org/10.1006/jmbi.1999.3268

Wieprecht T, Apostolov O, Beyermann M, Seelig J (2000) Interaction of a Mitochondrial Presequence with Lipid Membranes: Role of Helix Formation for Membrane Binding and Perturbation. Biochemistry 39:15297−15305. http://doi.org/10.1021/bi001774v

Wimley WC and White SH (1996) Experimentally Determined Hydrophobicity Scale for Proteins at Membrane Interfaces. Nat Struct Biol 3:842-848. https://doi.org/10.1038/nsb1096-842

Zhao H, Sood R, Jutila A, Bose S, Fimland G, Nissen-Meyer J, Kinnunen PK (2006) Interaction of the Antimicrobial Peptide Pheromone Plantaricin A with Model Membranes: Implications for a Novel Mechanism of Action. Biochim Biophys Acta 1758(9):1461-74. https://doi.org/10.1016/j.bbamem.2006.03.037

Figure Captions

Figure 1 – Isothermal titration calorimetry: a) Lipid-into-Pln149 titration of POPC (blue), POPG (red) and POPS (green), in aqueous solution and b) POPG with/without (grey/red) 250 mM NaCl. For the assays containing the salt solutions, the concentrations of the ions were the same in both liposome and peptide solutions at each measurement). The heat of injection obtained by integration of the heat flow peaks as a function of P/L molar ratio, at 25°C is shown in the lower diagram. In each measurement, 7 mM of vesicle suspensions were injected into a cell containing 28 μM of Pln149. Each peak refers to the injection of a 10 μl aliquot of the vesicles, which produced an endothermic heat of reaction. The first injection (only 2 μl injected) is prone to artifacts and was discarded from these analysis.

Figure 2 – Surface pressure studies: a) Surface activity of Pln149 (10 μM) on an air-water interface (black) and on monolayers of POPC (blue), POPG (red) or POPS (green) with lateral pressure of 25 mN/m, and b) adsorption of Pln149 (5 μM) onto POPC (blue), POPG (red), and POPS (green) monolayers. Lipid monolayers were formed at the air-water interface under different initial surface pressures (π_0), then peptide was injected into the water subphase. After equilibrium was reached, surface pressure changes ($\Delta\pi$), induced by Pln149 adsorption into each lipid monolayer were monitored.

Figure 3 – SRCD Spectroscopy: a) spectra of Pln149 in aqueous solution (black), in the presence of 10 mM of SDS (magenta), POPC (blue), POPG (red), and POPS (grey) vesicles at a 1/50 P/L molar ratio, and in a dehydrated film deposited on a quartz plate (green). b) Spectra of Pln149 in water (black) and in the presence of POPG (red) vesicles containing 0.25M (blue), or 0.5M (green) NaF. c) Helical wheel projection for the Pln149 sequence. Projection performed using residues A7 to K20, the region with a calculated helical propensity. Non-polar residues are labeled in yellow, positively-charged residues are in blue, and polar residues are in cyan.

Figure 4 – Oriented CD Spectroscopy: Pln149 as a function of P/L molar ratio in a) POPG (spectra were normalized to the sample of P/L 1:200, using the ellipticity value at 220 nm), b) POPS (spectra were normalized to the sample of P/L 1:100, using the value at 220 nm), and c) POPC (spectra were normalized to the sample of P/L 1:100, using the value at 220 nm) oriented bilayers. The dotted line indicates the wavelength at 208 nm, which is used for the OCD analyses.

Figure 5 – Optical Microscopy: Images of GUVs in the presence of Pln149 obtained using fluorescence (first and last images of each row) or phase contrast (middle images on each row) modes. Vesicle compositions and peptide concentrations are as follows: A- Giant vesicles composed of POPC (control); B- giant vesicles composed of POPC: POPG, 1:1 (control); C- giant vesicles composed of POPC: POPS, 1:1 (control); D- Giant vesicles composed of POPC with 64nM of Pln149; E- Giant vesicles composed of POPC: POPG (1:1) with 64 nM of Pln149; F- Giant vesicles composed of POPC: POPS (1:1) with 64 nM of Pln149.

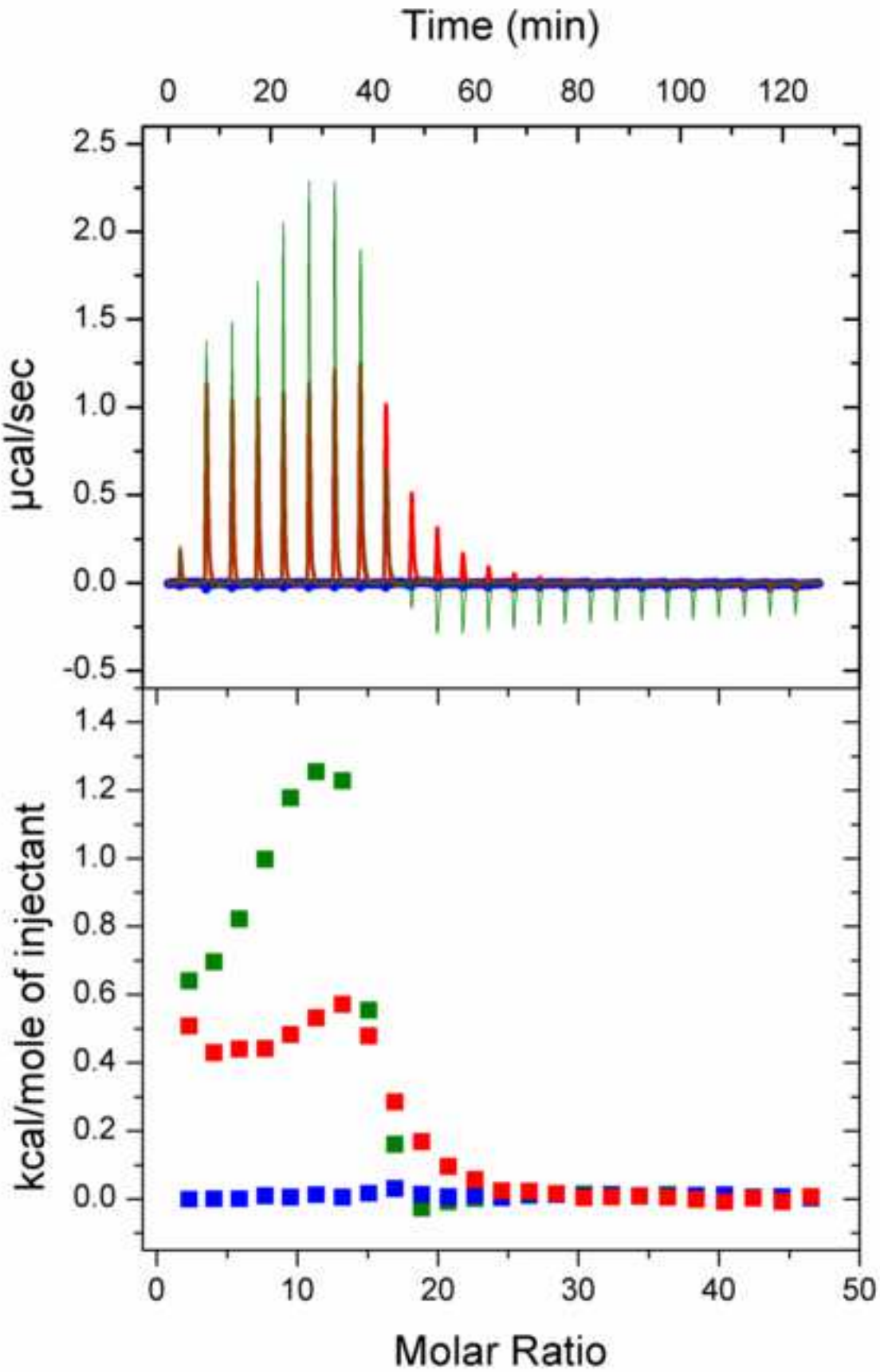

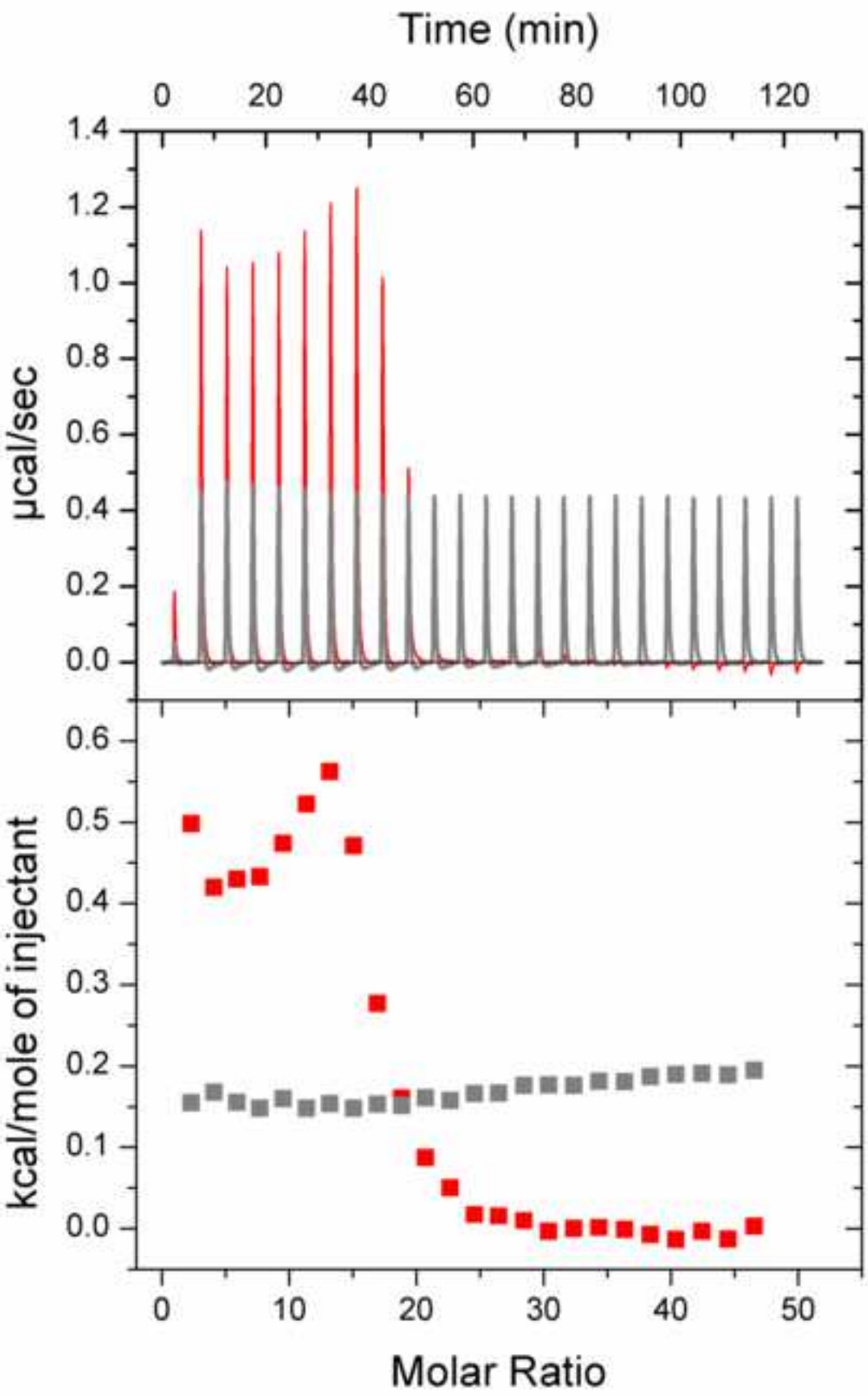

Fig2a

Click here to download Images Figure 2a.tif

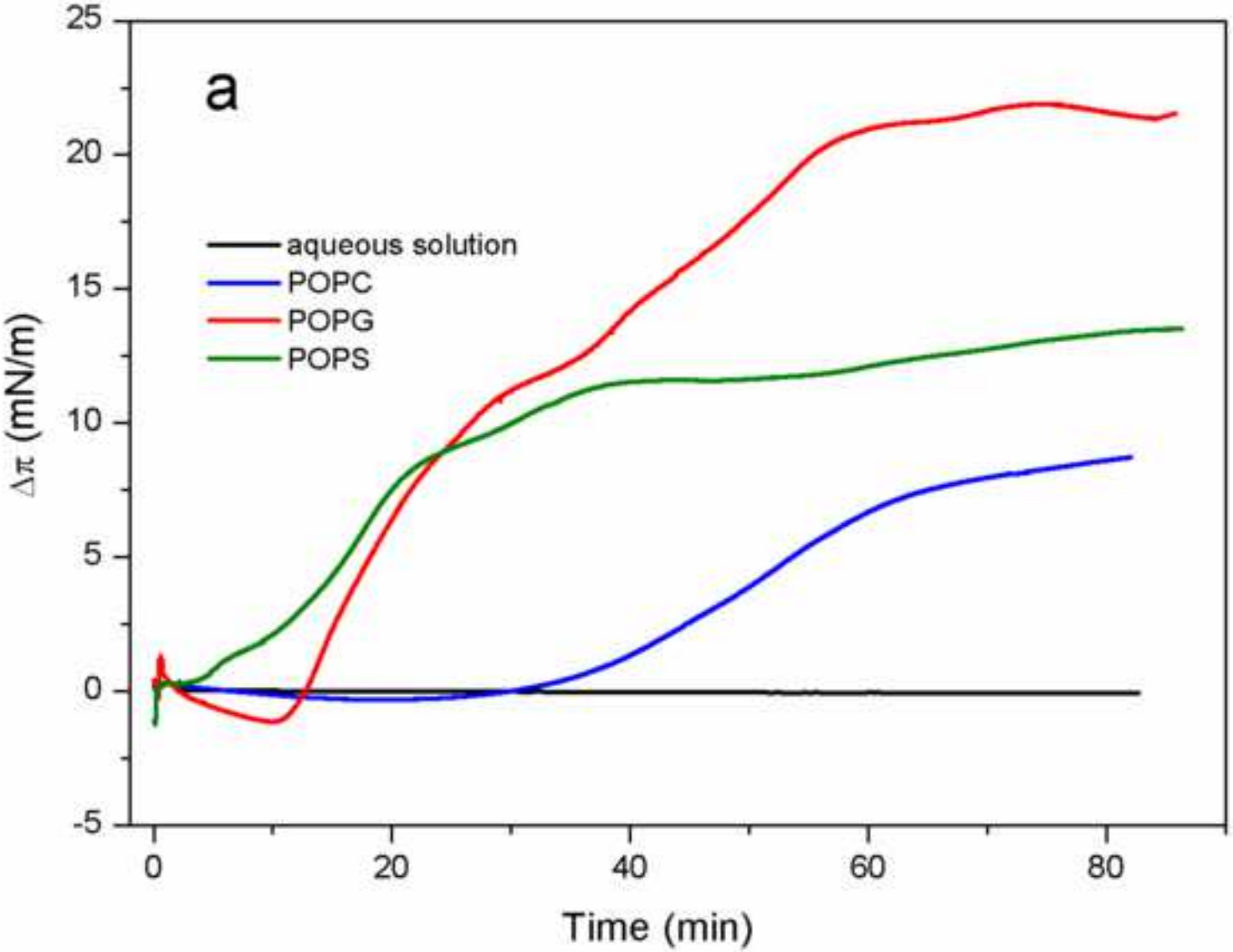

Fig2b

Click here to download Images Figure 2b.tif

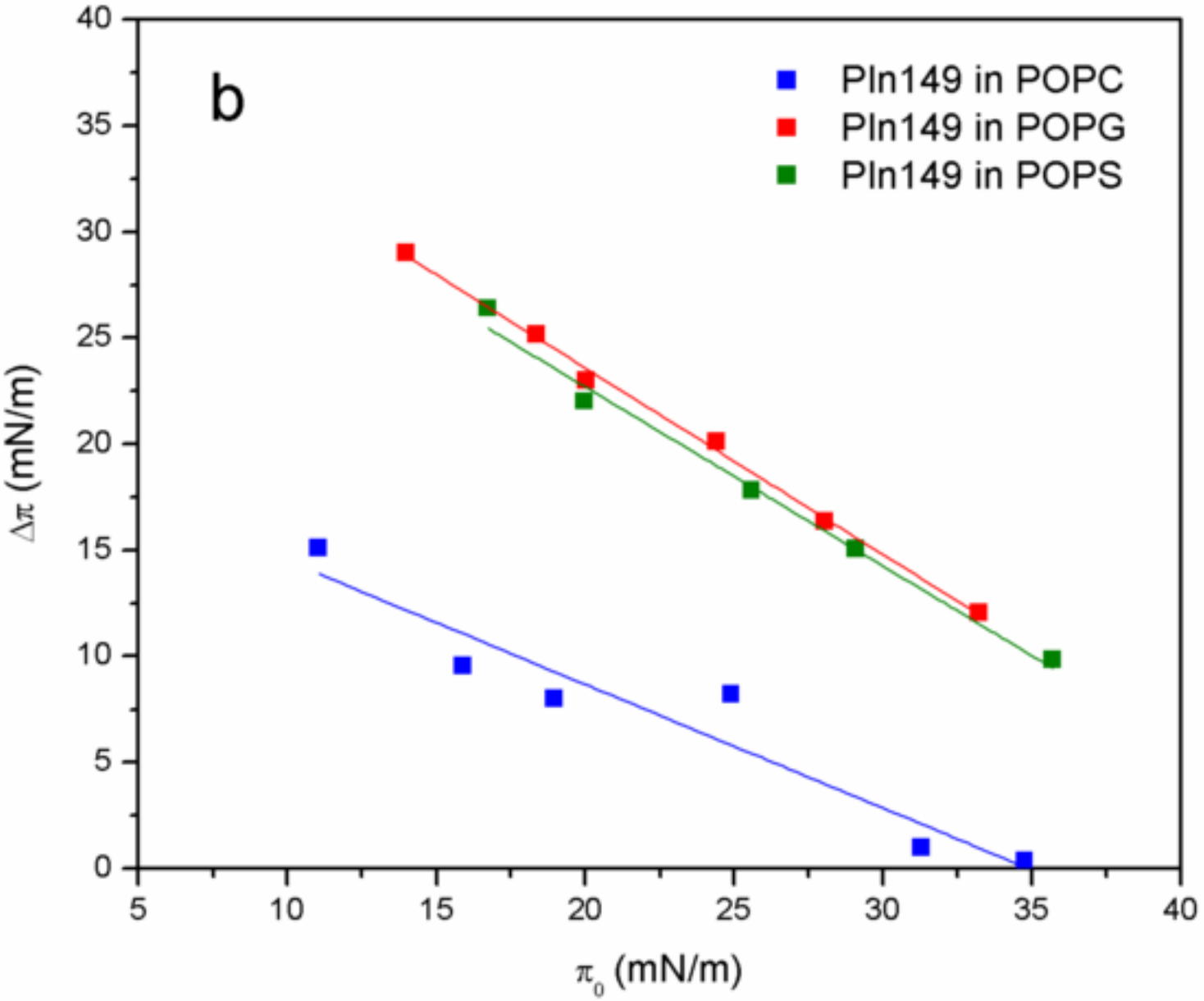

Fig3a

Click here to download Images Figure 3a.tif

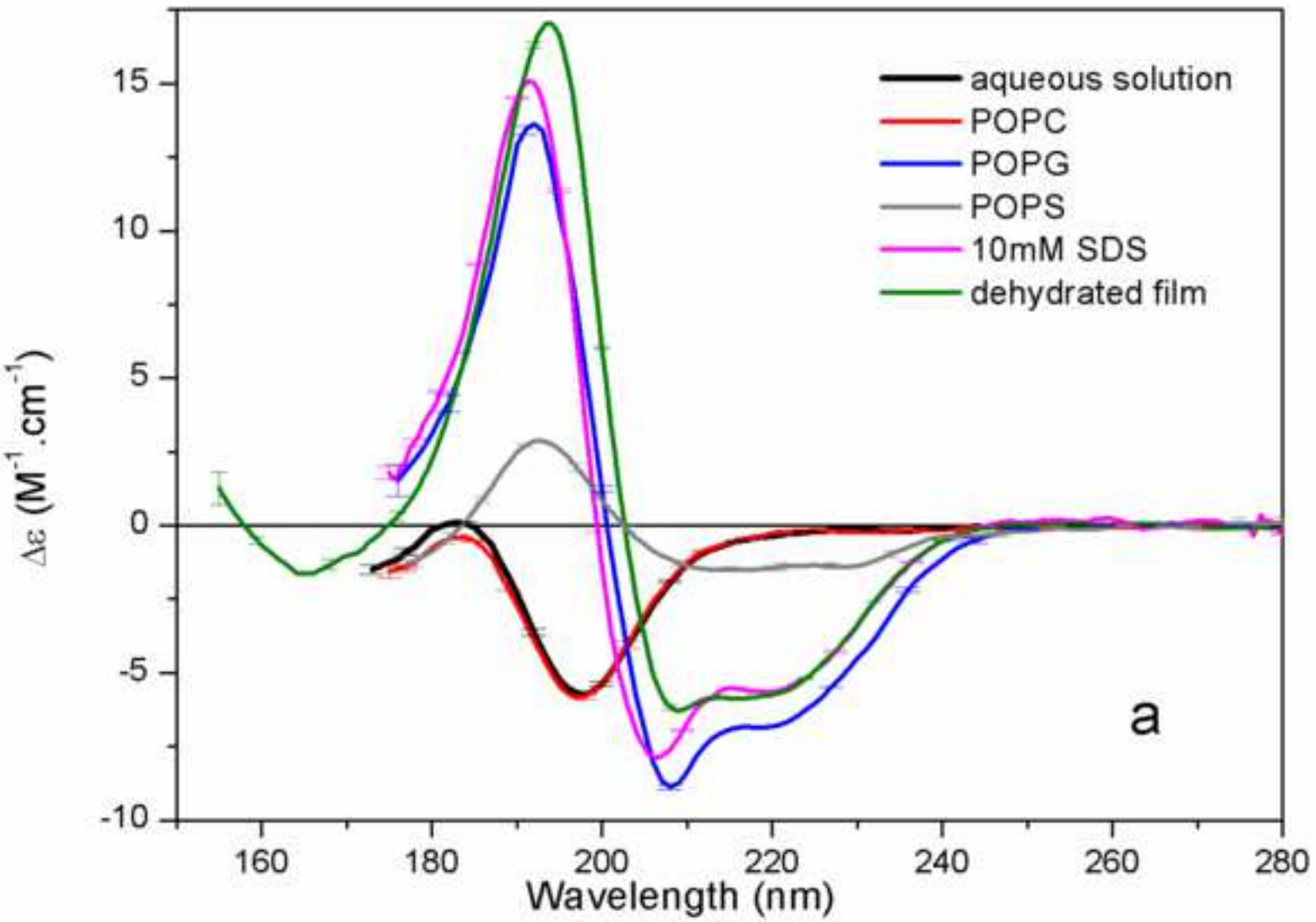

Fig3b

Click here to download Images Figure 3b.tif

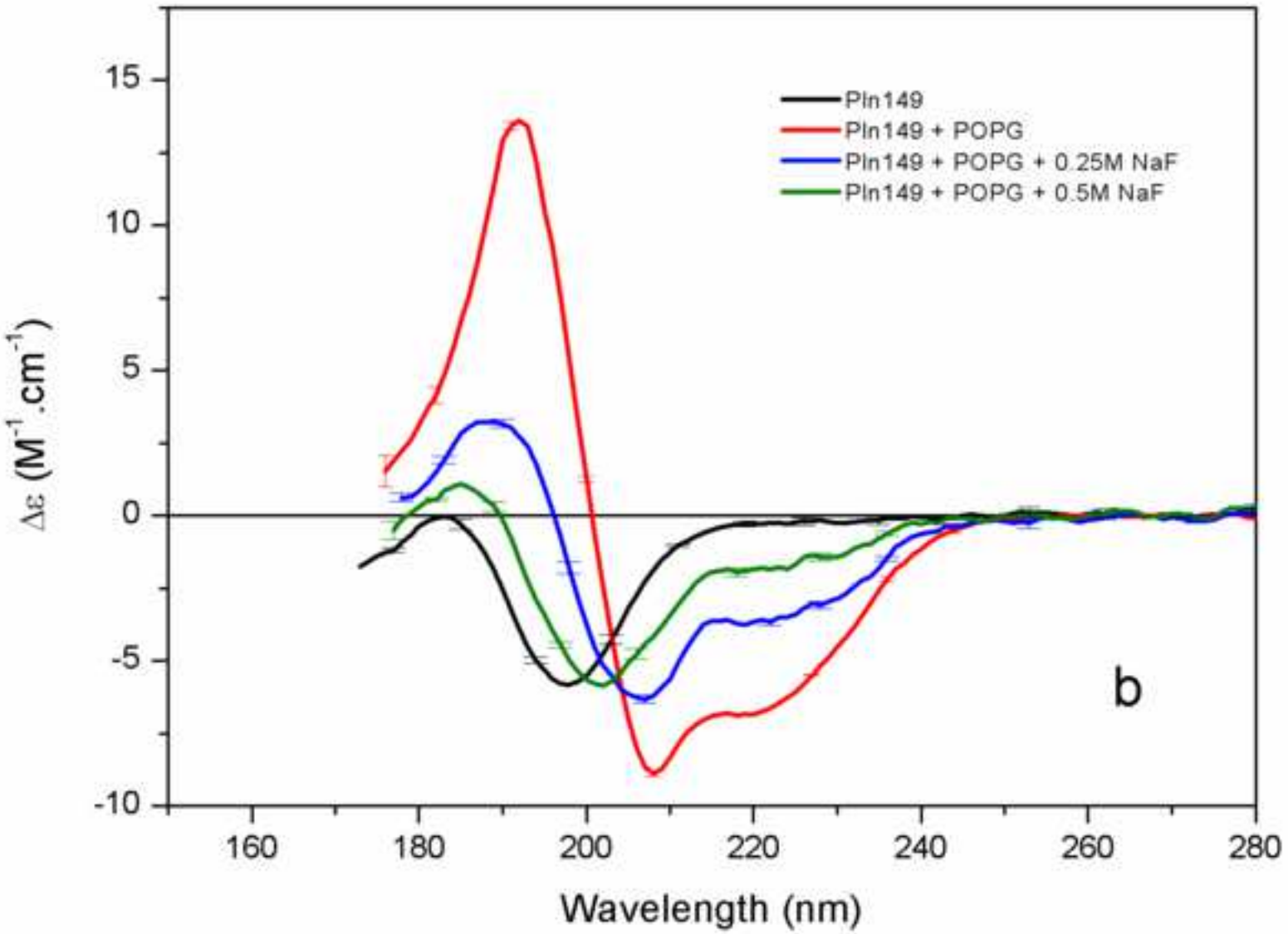

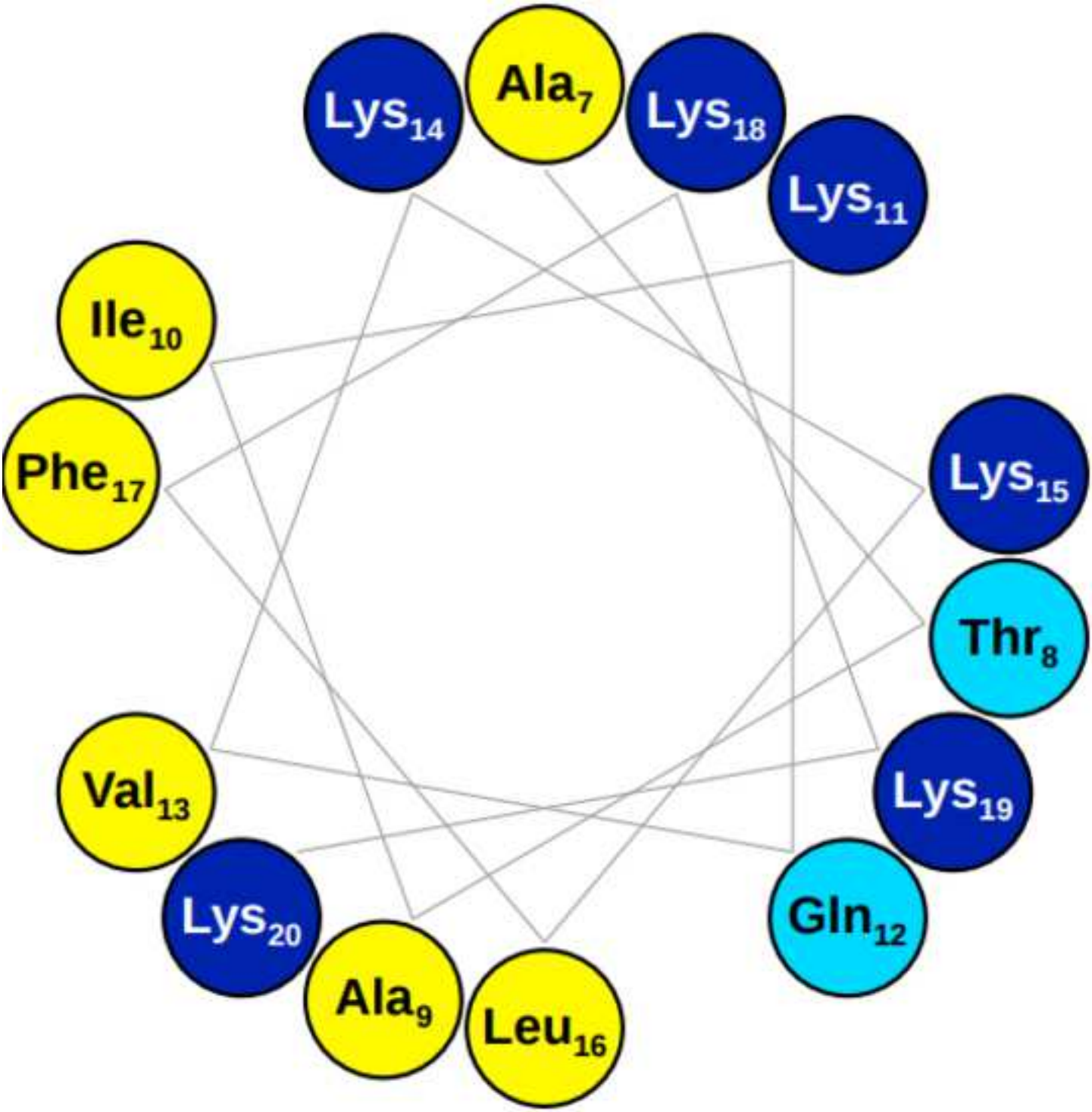

Fig4a

Click here to download Images Figure 4a.tif

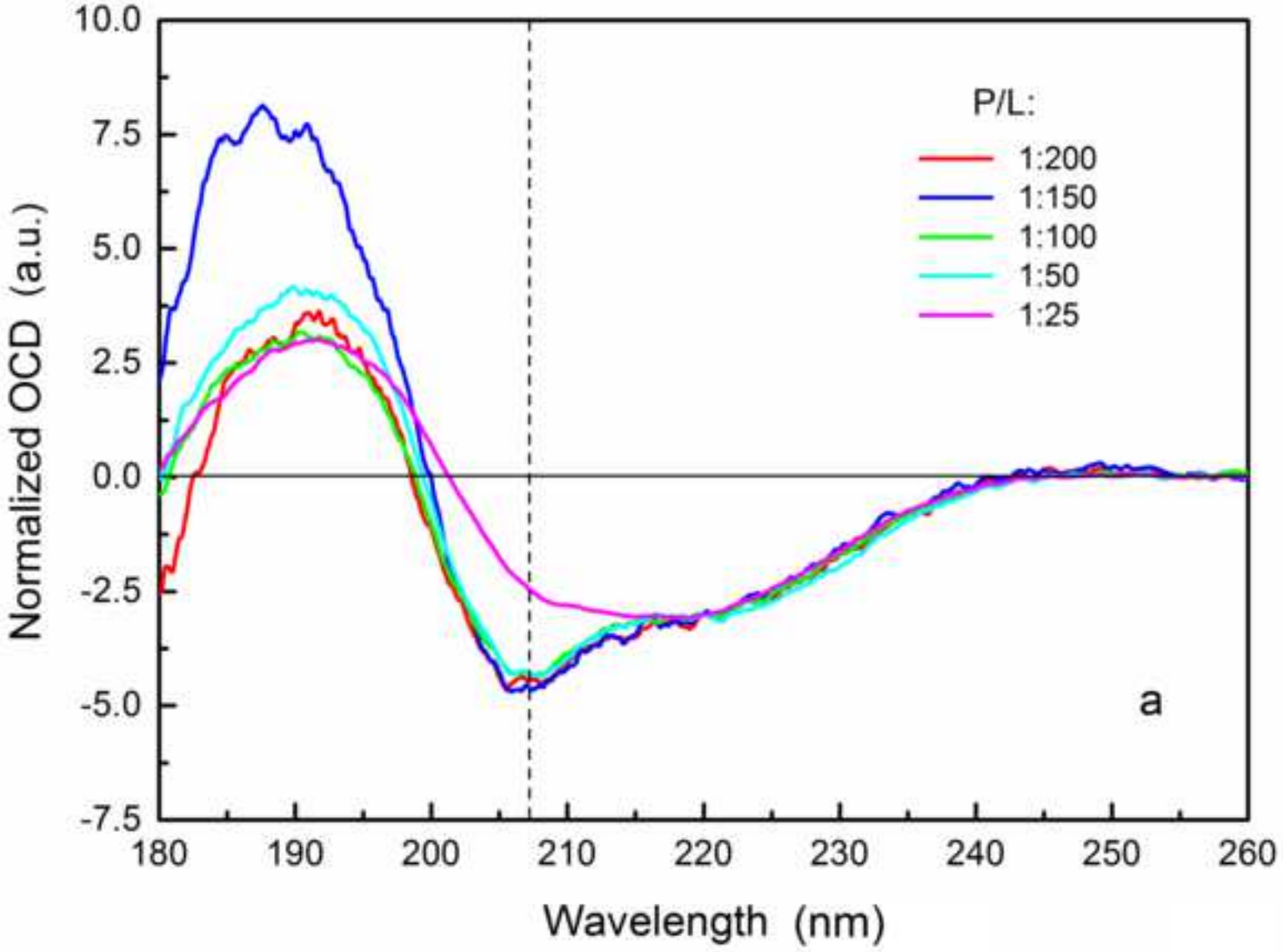

Fig4b

Click here to download Images Figure 4b.tif

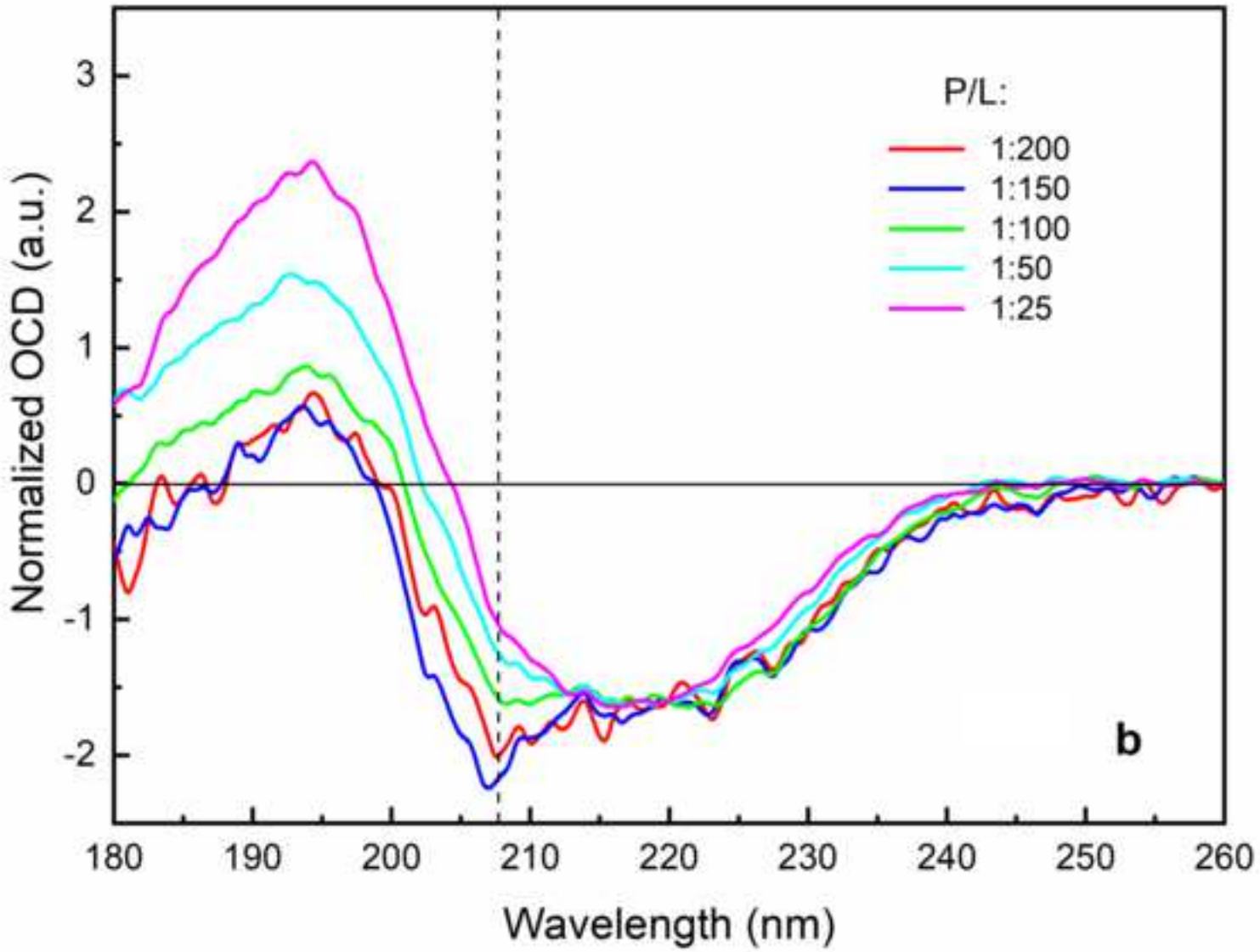

Fig4c

Click here to download Images Figure 4c.tif

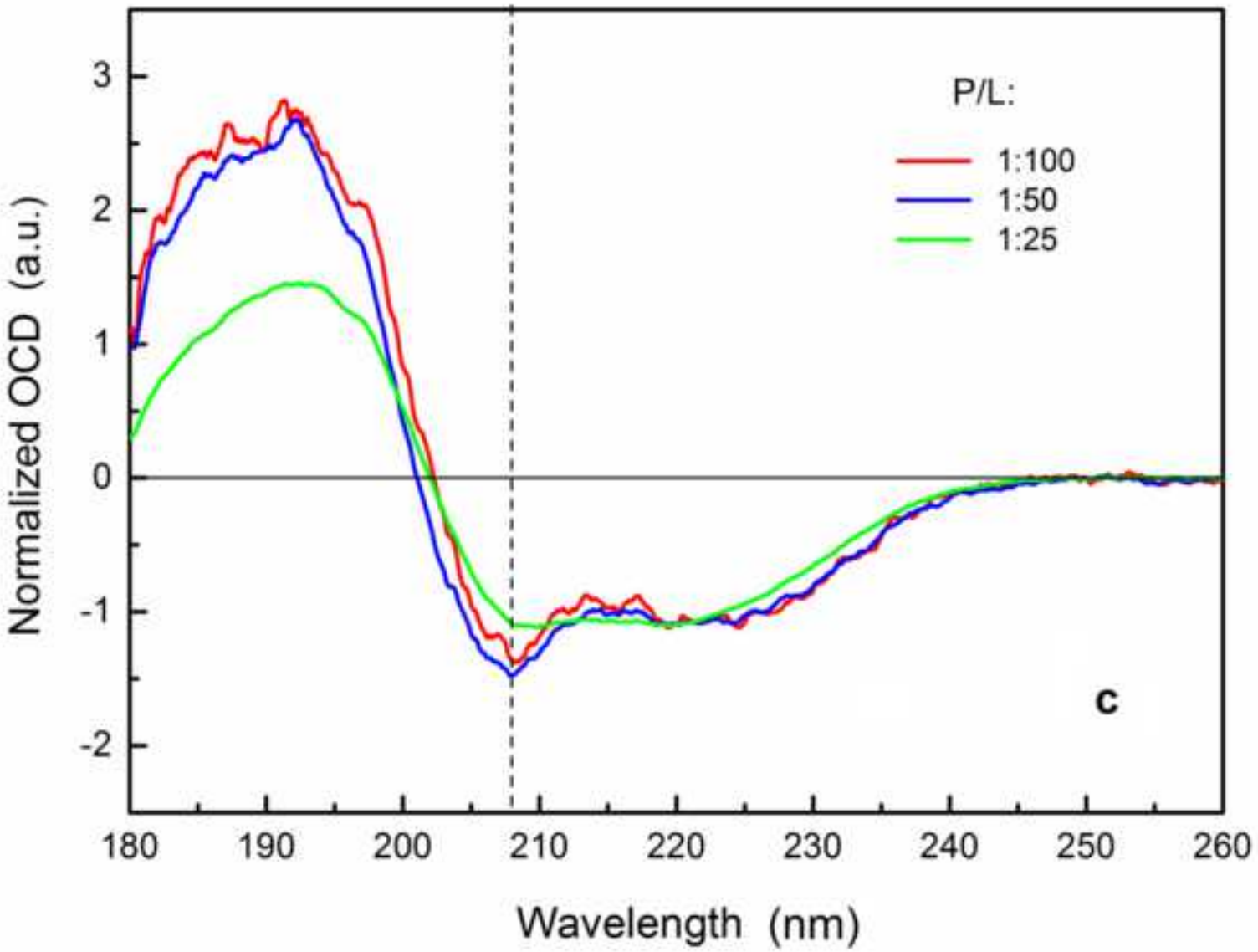

Fig5

Click here to download Images Figure 5.tif